Heritable yeast prions have a highly organized three-dimensional architecture with interfiber structures

Helen R. Saibil[a,1], Anja Seybert[b], Anja Habermann[b], Juliane Winkler[c], Mikhail Eltsov[b,d], Mario Perkovic[b], Daniel Castaño-Diez[d,2], Margot P. Scheffer[b,d], Uta Haselmann[d], Petr Chlanda[d,3], Susan Lindquist[e,1], Jens Tyedmers[c,1], and Achilleas S. Frangakis[b,d,1]

[a]Crystallography and Institute for Structural and Molecular Biology, Birkbeck College, London WC1E 7HX, United Kingdom; [b]Institut für Biophysik and Frankfurt Institute for Molecular Life Sciences (FMLS), Johann Wolfgang Goethe Universität, D-60438 Frankfurt, Germany; [c]Center for Molecular Biology of the University of Heidelberg and German Cancer Research Center, DKFZ-ZMBH Alliance, Universität Heidelberg, D-69120 Heidelberg, Germany; [d]European Molecular Biology Laboratory (EMBL), D-69117 Heidelberg, Germany; and [e]Whitehead Institute and Howard Hughes Medical Institute (HHMI), Department of Biology, Massachusetts Institute of Technology, Cambridge, MA 02142

Contributed by Susan Lindquist, July 18, 2012 (sent for review June 3, 2012)

Yeast prions constitute a "protein-only" mechanism of inheritance that is widely deployed by wild yeast to create diverse phenotypes. One of the best-characterized prions, [*PSI*$^+$], is governed by a conformational change in the prion domain of Sup35, a translation-termination factor. When this domain switches from its normal soluble form to an insoluble amyloid, the ensuing change in protein synthesis creates new traits. Two factors make these traits heritable: (*i*) the amyloid conformation is self-templating; and (*ii*) the protein-remodeling factor heat-shock protein (Hsp)104 (acting together with Hsp70 chaperones) partitions the template to daughter cells with high fidelity. Prions formed by several other yeast proteins create their own phenotypes but share the same mechanistic basis of inheritance. Except for the amyloid fibril itself, the cellular architecture underlying these protein-based elements of inheritance is unknown. To study the 3D arrangement of prion assemblies in their cellular context, we examined yeast [*PSI*$^+$] prions in the native, hydrated state in situ, taking advantage of recently developed methods for cryosectioning of vitrified cells. Cryo–electron tomography of the vitrified sections revealed the prion assemblies as aligned bundles of regularly spaced fibrils in the cytoplasm with no bounding structures. Although the fibers were widely spaced, other cellular complexes, such as ribosomes, were excluded from the fibril arrays. Subtomogram image averaging, made possible by the organized nature of the assemblies, uncovered the presence of an additional array of densities between the fibers. We suggest these structures constitute a self-organizing mechanism that coordinates fiber deposition and the regulation of prion inheritance.

Prions are self-replicating protein conformations found in yeast, fungi, and mammals. A nearly universal feature of prions is a conformational switch that converts a normally soluble, monomeric protein into a fibrous assembly with a cross–β-amyloid structure. Prions have the additional property of "infectivity," with the prion amyloid conformation catalyzing conformational conversion of the normal soluble form of the protein.

In mammals, conversion of a prion protein, PrP, to its infectious Prp^{Sc} conformation is the basis of transmissible spongiform encephalopathies, in which spreading of Prp^{Sc} kills neurons by mechanisms that still remain elusive (1). Heightening interest in this process, proteins involved in several other neurodegenerative diseases have recently been shown to propagate in a prion-like manner, and this activity is likely to play an important role in determining the pathogenic properties of these proteins (2).

Remarkably, prions can play important roles in normal biological processes (3, 4). In metazoans, prion-like conformational switches function in processes as diverse as the maintenance of neuronal synapses (5, 6) and antiviral immunity (7). In fungi, prions provide a paradigm-shifting mechanism for the inheritance of biological phenotypes: the prion conformational change produces a change in function that is inherited through the transmission of a self-perpetuating protein conformation rather than through transmission of altered nucleic acids (3, 4, 8).

Nearly a dozen yeast proteins are now known to switch into prion states. Most of them are hubs of cell regulation, and their prion states have a major impact on cell phenotype (3, 4, 9–11). Many more potential prion proteins have been discovered recently (12). Several of these, as well as the factors that regulate them, have been conserved for hundreds of million years (5, 13–15). Moreover, it has been discovered that yeast prions are widespread in nature, where they confer many phenotypes that have clear adaptive value (8). One of the most remarkable features of prion biology is their ability to link biological stresses to heritable changes in phenotype. This is a natural consequence of the effect of such stresses on protein homeostasis (3, 16–18). We are still, however, at an early stage in understanding the mechanisms by which these protein-based elements of inheritance are propagated. Here, we apply recently developed imaging methods to one of the best-characterized yeast prion proteins, Sup35.

Sup35 forms the prion known as [*PSI*$^+$]. (The brackets denote its nonchromosomal, cytoplasmic inheritance, and the capital letters denote its dominant behavior in genetic crosses.) The protein has a C-terminal GTPase domain that normally functions as a translation termination factor. Two other domains govern the ability of Sup35 to switch between a stable functional state and a stable nonfunctional prion state. The middle region, M, is highly charged and helps maintain the soluble nonprion state. The N-terminal region, N, that is strongly enriched in asparagine and glutamine, is amyloidogenic, and promotes prion formation (5, 11, 19, 20). Importantly, the conformational transitions of

Author contributions: H.R.S., S.L., J.T., and A.S.F. designed research; H.R.S., A.S., A.H., J.W., M.E., M.P., D.C.-D., M.P.S., U.H., P.C., J.T., and A.S.F. performed research; H.R.S., J.T., and A.S.F. analyzed data; and H.R.S., S.L., J.T., and A.S.F. wrote the paper.

The authors declare no conflict of interest.

Freely available online through the PNAS open access option.

Data deposition: The data reported in this paper have been deposited in the Electron Microscopy Data Bank (EMDB), www.ebi.ac.uk/pdbe/emdb (accession nos. EMD-2103 and EMD-2104).

[1]To whom correspondence may be addressed. E-mail: h.saibil@mail.cryst.bbk.ac.uk, lindquist_admin@wi.mit.edu, j.tyedmers@zmbh.uni-heidelberg.de, or frangak@biophysik.org.

[2]Present address: Center for Molecular Life Sciences, Biozentrum, University of Basel, CH-4058 Basel, Switzerland.

[3]Present address: Section on Membrane and Cellular Biophysics, National Institute of Child Health & Human Development, National Institutes of Health, Bethesda, MD 20892.

This article contains supporting information online at www.pnas.org/lookup/suppl/doi:10.1073/pnas.1211976109/-/DCSupplemental.

NM are sufficient to explain all of the essential features of prion induction, propagation, and inheritance (5, 21–25).

Prions formed by NM, and most other yeast prions, engage the protein remodeling activities of heat-shock protein (Hsp)104, a hexameric AAA+ ATPase, in their propagation (5, 11, 21, 26). Hsp104 acts on NM in several distinct ways (27), but a critical function is amyloid fiber severing that allows partitioning of the prions to daughter cells (28–31). Several other factors, including protein chaperones in the Hsp70 and Hsp40 families, proteins connected to the cytoskeleton, and proteins involved in the partitioning of other types of protein aggregates, copurify with the prions (32–37) and influence their inheritance in ways that are only partially characterized (4, 11, 38).

We and others (21, 29, 33, 35–37, 39–42) have used fusions between the Sup35 NM domain and GFP to visualize various aspects of prion inheritance. This creates a prion with all of the biochemical and genetic properties of [*PSI*$^+$], except that it is fluorescent. When the NM domain is deleted from the endogenous copy of Sup35, this protein can be overexpressed, with no effects on translation. Overexpression greatly increases the rate of de novo prion induction, allowing visualization of what is normally a very rare event. Such work led to identification of a "transition state" during prion induction (33, 35–37, 39, 41) that is characterized by the appearance of large rings, or ribbons of NM amyloid fibers, hereafter referred to as "rings." These contain long continuous bundles of NM fibers and propagate faithfully for many generations before maturing into an infectious prion state, in which cells display a single large, dot-shaped aggregate composed of short amyloid fibrils. The amyloid fibers in rings have the same biochemical properties as those in dots. Furthermore, lysates from both cell types can template conversion of soluble recombinant NM in vitro into fibers that have the same ability to transform prion-minus cells to [*PSI*$^+$]. However, cells with rings do not propagate the "infectious" prion state to mating partners, whereas cells with dots do (35). This is consistent with the notion that fiber ends generate the infectious "propagons" (43) via the amyloid-severing activity of Hsp104, with the assistance of the other cellular factors (28, 30, 31, 41, 44).

Overexpression of NM-GFP also creates a much larger prion assembly, the structure of which can be readily investigated by both light and electron microscopy (EM). Here, we use high-pressure freezing, cryosectioning, and cryo–electron tomography to examine the 3D structure of these assemblies in their native, hydrated cellular states. Alignment and averaging of fiber segments extracted from the tomograms unexpectedly revealed additional, discrete structures intercalated between the fibrils. Fluorescence microscopy with tagged proteins reveals a variety of chaperones present in the fiber arrays, and components of the Hsp70 system are potential candidates for the additional structures. We suggest the highly ordered arrays of fibers and intercalated structures described here reflect an underlying organization common to the smaller propagons of prion-based inheritance. The parallel in-register organization of *Drosophila* polytene chromosomes provided early insights into chromosome organization impossible to discern in somatic chromosomes by early light microscopy techniques. In the present work, the higher-order organization of this prion-based genetic material has enabled us to locate and characterize previously unknown substructures using current methods of electron tomography.

Results

Three-Dimensional Arrangement of NM-GFP Fibrils in Ring and Dot Assemblies. To study the structure and organization of amyloid aggregates in vivo, we expressed the Sup35 prion domain NM, fused to GFP or YFP, at high levels in cells lacking the NM prion domain in their endogenous SUP35 gene (*SI Materials and Methods*). This prevents any toxicity associated with Sup35 sequestration, because the C-terminal domain is immune to sequestration (45). We used high-pressure freezing and freeze substitution to prepare stained, resin-embedded sections with excellent preservation of cellular structure (*SI Materials and Methods*). We used electron tomography to determine the 3D structures of the fiber aggregates in ring and dot cells (Fig. 1). As reported previously with conventional EM (35, 41),

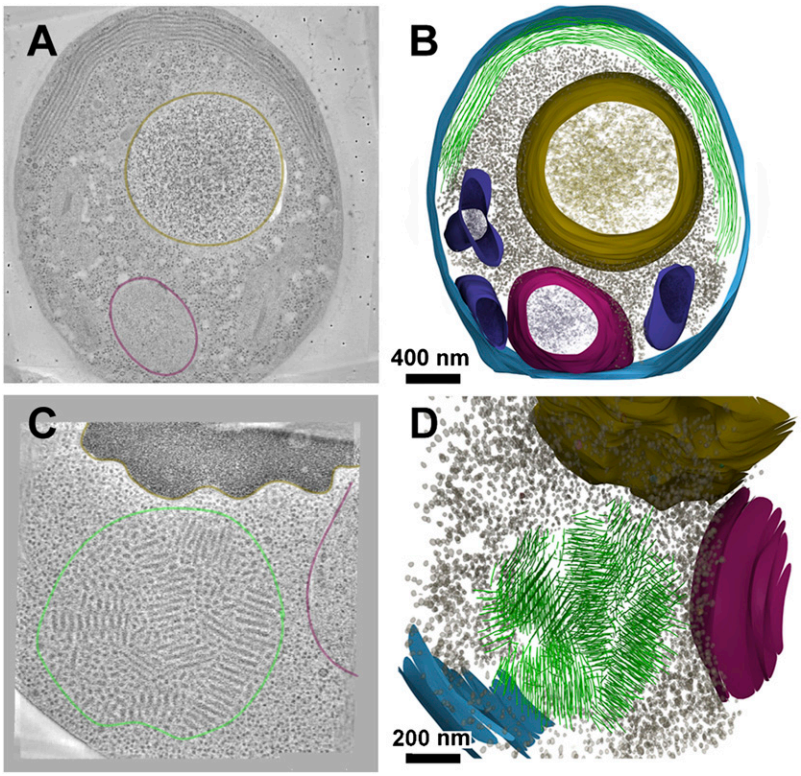

Fig. 1. Three-dimensional analysis of ring and dot structures in freeze-substituted yeast cells. (*A*) Section through a tomogram of a ring cell, with about half of the ring in the plane of the section. The nucleus is outlined in magenta and the vacuole in brown. (*B*) Rendered 3D model from serial tomograms of this ring cell. Ring fibers are in green; membrane, blue; nucleus, magenta; vacuole, brown; mitochondria, purple; and large complexes (presumably ribosomes) as gray dots. The large complexes in the cytoplasm are excluded from the fiber area. (*C*) Section through a dot cell tomogram, colored as above. (*D*) Rendered 3D model of the dot from serial tomograms, showing the mosaic arrangement of fiber bundles. (Coloring as in *B*.)

the rings contained long fibers, and the dots were formed by a mosaic of short fibril bundles. Both ring and dot fibrils were packed in aligned bundles, with a center-to-center spacing of ~34 nm. In this stained material, the diameter of the fibril itself was ~25 nm.

To trace the fibril paths, we used serial tomography covering most or all of several dot structures and most of one ring. Strikingly, in all images, we found no discontinuities in hundreds of ring fibers examined, except for those located at the artificial boundaries between successive cut sections. That is, the fibers of ring cells were continuous. Typical views of fibril packing are shown in a cell section with NM-GFP rings (Fig. 1*A*), and a rendered model of the cell is shown in Fig. 1*B*. A section and rendered model of a cell containing an NM-GFP dot are shown in Fig. 1 *C* and *D*. A movie of the dot fiber model, constructed from seven serial sections of one cell is shown in Movie S1.

The width of fiber bundles in cells with NM-GFP rings was ~200 nm. Dot bundles ranged up to ~700 nm in width. The individual fibers in rings were very long, averaging several microns in length. Dot fibrils were much shorter, with many fiber ends. The fibrils of ring and dot cells have the same biochemical properties (35). Indeed, lysates made from such cells have equivalent capacities to seed the polymerization of purified NM, and such preparations, in turn, have equivalent capacities to transform [*psi*$^-$] cells to [*PSI*$^+$] by protein-only transformation. Biologically, ring and dot cells are distinguished only by the fact that ring cells cannot transfer the prion state to [*psi*$^-$] mating partners and are, therefore, not "infectious." Thus, tomography provides independent support for the hypothesis that fiber ends are the source of infectious propagons in vivo (41).

Notably, the lengths of fibrils in dot structures fit to a normal distribution, with a peak at 110 nm (Fig. S1 *A* and *B*). Thus, it seems that the infectious dot arrays are not simply formed by random cleavage of fibers in the ring bundles. Rather, to account for their relatively uniform length, there must be a concerted mechanism for growth, lateral interaction, and fiber cleavage in these cells.

Fibril Arrays in Ring and Dot Assemblies Are Attributable to the Prion Domain. GFP retains its fluorescence in ring and dot assemblies (29, 33, 35, 39, 41). It must, therefore, be natively folded when incorporated in these fibrils. Because our interest was in discerning architectural elements characteristic of prion-based mechanisms of inheritance, it was important to ensure that the spatial organization and structural features of these assemblies were dictated by the prion domain and not by GFP. We prepared cells expressing NM from the same overexpression plasmid with an HA, myc or FLAG tag, but no GFP, downstream of NM (*SI Materials and Methods*). Freeze-substituted sections of the HA-tagged fibrils showed the same interfibril spacing (~31 nm; Fig. S2*A*). Thus, the observed fibril packing is dictated by the NM prion domain and any associated cellular factors, not by GFP.

NM-GFP Fibrils Do Not Maintain Associations with the Preautophagosomal Structure. Previously, the NM-GFP plasmid used in our studies was used to envision early events in prion induction, which are too rare to capture in the absence of overexpression. Conversion events were associated with an ancient system for the asymmetric inheritance of damaged proteins at the rim of the vacuole, at a site adjacent to the preautophagosomal structure (PAS) (35) known as the Insoluble Protein Deposit (IPOD) (46). This site is also associated with accumulations of Rnq1 (35, 46), a factor that promotes prion induction (42, 47). We, therefore, examined established NM fibril bundles for associations with the vacuolar rim. In some fibril dot structures, a minimal contact site was seen, at which one or a few fibrils at the edge of the dot were directly adjacent to the vacuole surface, excluding the otherwise ubiquitous ribosomes from the putative contact region. In serial reconstructions of other dots, no contact with the vacuole was seen. No direct contact with the vacuole was observed in the ring cell shown in Fig. 1 *A* and *B*. Therefore, we conclude that direct contacts with the vacuolar rim are not essential for maintenance of the dots or rings, although they are observed in some cases.

Cryo–Electron Tomography to Characterize Native, Hydrated Fibril Assemblies in Situ. To examine the fibril assembly in the absence of potential artifacts caused by staining and dehydration, we used cryo–electron tomography of vitrified sections. In this approach, the unfixed, high-pressure frozen cells are sectioned in the vitreous state and viewed by cryomicroscopy with liquid nitrogen cooling and without thawing, fixation, or staining (48). Therefore, the material remains in the native hydrated state. Under these conditions, fibrils appeared thinner than in the stained, freeze-substituted sections (10 nm), and their center-to-center distance was more variable in the cryosections (25–50 nm) (Fig. 2). This may be attributable to mechanical section compression, but we did not observe a direct relationship between the sectioning direction and the interfiber spacing. An alternative explanation for the observed variable spacing is that the apparent separation distance depends on the oblique orientations of the fibrils in these 50- to 80-nm-thick sections. The core fibril diameter was consistent with EM studies of full-length, NM- and N-domain fibrils in vitro, which showed that the middle and C-terminal domains are flexible and can extend considerably from the fibril backbone (49). By analogy, it is likely that the globular GFP domains are also mobile in our fibrils. As noted above, a similar fibril spacing was observed with constructs lacking GFP, demonstrating that these properties were attributable to

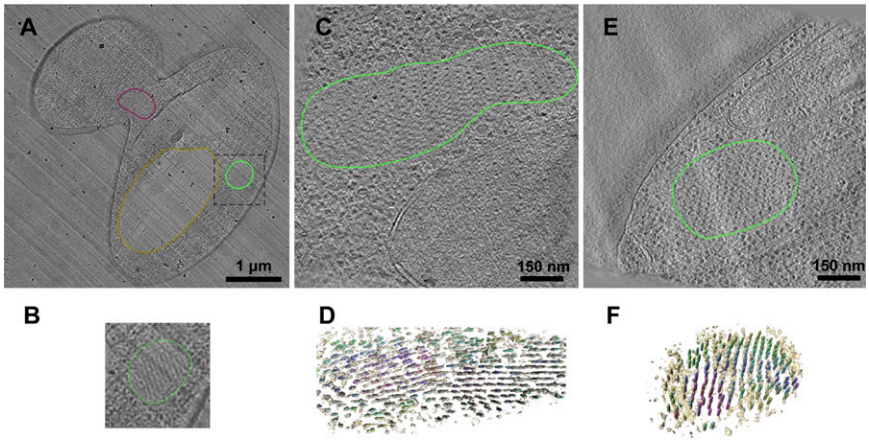

Fig. 2. Cryosections of dot and ring cells. (*A*) Overview section of a budding yeast cell with a dot aggregate, outlined as in Fig. 1. The cell is compressed along the direction of sectioning, indicated by the knife marks (diagonal streaks). (*B*) Enlargement of the dot region. (*C*) Tomogram slice of a ring, adjacent to the nucleus. (*D*) Rendered views of the fibers in the ring, colored by their cross-correlation values, with the most ordered regions in purple and least ordered in yellow. (*E*) Tomogram slice of a dot cell. (*F*) Rendered view of the fibril array in the dot, colored as in *D*.

fundamental organizing principles of the prion domain and its association with other cellular factors (Fig. S2*A*).

Subtomogram Averaging Reveals Additional Structures Intercalated Between the Fibrils. Two striking features of the assemblies revealed by electron tomography are: (*i*) the exclusion of other cytoplasmic contents, such as the normally ubiquitous and abundant ribosomes, despite the wide separation between fibrils; and (*ii*) the alignment of fibrils in arrays (Fig. 1). These observations suggest the presence of additional cellular components between the fibril cores, factors that might act to exclude ribosomes and to align the fibrils into small arrays. To investigate the 3D structural organization of these assemblies in more detail, we used subtomogram averaging, a single-particle approach in which small 3D subregions of the fibril lattice are extracted from a tomogram, aligned, classified, and averaged in 3D, to improve the signal to noise ratio and reveal more structural detail.

Overviews of a ring and dot lattice analyzed in this manner are shown in Fig. 3 *A* and *B*, respectively. The fibrils are arranged in a quasiordered lattice, with several shells of neighboring fibrils revealed by the subtomogram averaging, as seen in the resin-embedded sections. Remarkably, the averaging clearly revealed additional structures between the fibrils. Elongated densities surrounded and extended from the fibrils (Fig. 3 *C–F*). The additional features were each ~8- to 9-nm in length. The most detailed average was obtained from the ring assemblies, in which the fibrils were aligned more nearly parallel to the section plane. However, similar structures were also seen, at lower resolution, after image averaging of dot assemblies (Fig. 3 *G–J*). Although the interfibril structures do not appear to be strongly connected to the fibers, the level of defocus needed to give sufficient contrast in cryosections causes a halo of lower density around high-density features such as the fibrils. Therefore, a direct contact between the individual fibers and the newly identified interfibril structures is depicted in the illustration in Fig. 3*K*. The presence of six to seven discrete densities surrounding the fiber in the subtomogram average indicates that they are ordered, repeating structures in the fiber array (Fig. 3 *A* and *B*). The reliability of the averaged maps is supported by the appearance of two to three shells of neighboring fibers, because these surrounding structures were not present in the reference image that was generated from the central fiber and used for alignment. These additional structures could explain the wide fiber spacing and exclusion of cytoplasmic components in between the fibers. It is likely that interfiber contacts would underlie the observed, ordered arrangement of fibers into arrays.

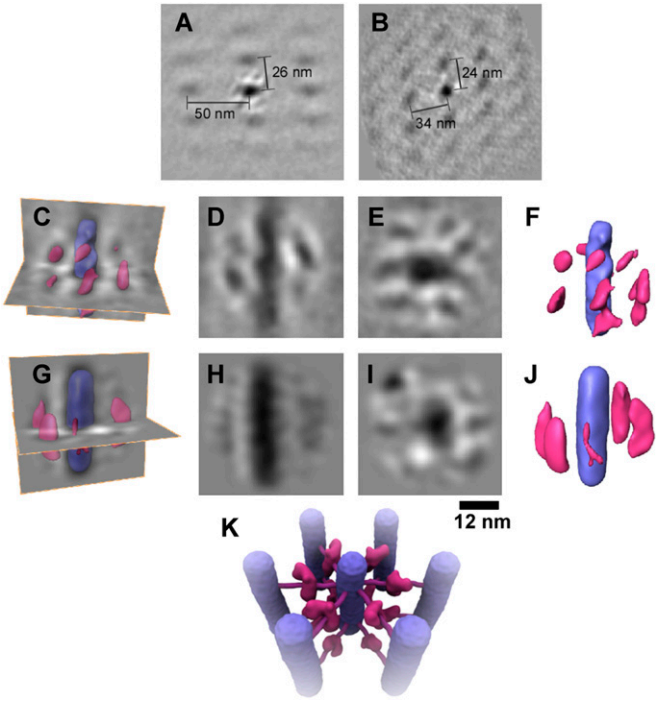

Fig. 3. Subtomogram averages of the fiber arrays. Subregions of the cryotomograms were aligned and averaged to reveal additional structures surrounding the fibers. (*A*) Section through the array of ring fibers, with the region in the center showing the averaged density surrounded by the array of fibers. (*B*) Equivalent view of the dot fiber array. The variable spacing might arise from sectioning artifacts and/or oblique fibril orientations. (*C*) Rendered views of the ring average superposed on density sections. (*D* and *E*) Long- and cross-sections of the averaged ring fiber. (*F*) Rendered view of the averaged fiber with the surrounding structures. The fiber is shown in purple and the additional structures in pink. (*G*) Rendered view of the dot average superposed on density sections as above. (*H* and *I*) Long- and cross-sections of the dot fiber average. (*J*) Rendered view of the averaged fiber with the surrounding structures, colored as in *F*. The differences in dot and ring structures most likely arise from the lower resolution obtained for the dot average. The defocus needed to obtain sufficient contrast in cryosections causes a white halo around high-density (dark) features; therefore, obscuring regions of contact between the central fiber and surrounding structures. (*K*) Illustration of the deduced arrangement of cross-bridges between the fibers. Fibers are in purple, and cross-bridge structures are in pink.

Molecular Chaperones Are Abundant Components of the Fiber Assemblies and Can Influence Their Structural Organization. As an initial approach to identifying the interfibrillar structures, we probed factors known previously to interact with prions and influence their inheritance. The model derived from our subtomogram averaging predicts that molecules forming these interfibrillar structures should be present at a similar level as NM-YFP. In a quantitative study, Bagriantsev et al. (34) found the Hsp70 proteins Ssa1 and Ssa2 in a ~1:1 ratio, with Sup35 in prion aggregates from [*PSI*$^+$] cell lysates, along with other less abundant proteins, such as additional molecular chaperones implicated in prion biology (26, 31, 32, 44, 50–53), for example Sis1 and Hsp104, and a protein known to regulate actin dynamics during endocytosis, Sla2 (33, 36).

Therefore, we asked whether molecular chaperones and protein remodeling factors are components of the assembly. We tagged the genomic copies of Ssa1 and Ssa2 and the Hsp40/J protein Sis1, as well as Hsp104 and Hsp110 (a member of the Hsp70 family known as Sse), with CFP in cells that were expressing NM-YFP (*SI Materials and Methods*). The shift from NM-GFP to YFP was made simply to allow separation of its fluorescent signal from that of CFP. All of these proteins colocalized with both rings and dots (Fig. 4).

To further investigate the role of Hsp70 proteins and to determine whether genetic manipulations of yeast might provide tools for future analyses of prion cytoarchitecture, we used a [*PSI*$^+$] strain deficient in Hsp70. Hsp70 proteins are redundant in all eukaryotes, and in yeast, four genes encode the family of Hsp70s in the cytosolic and nuclear compartments (known as Ssa proteins). We used a strain in which three of the four Ssa proteins were deleted (Ssa2–4Δ) and the single remaining Ssa member, Ssa1, was replaced by a temperature-sensitive (ts) mutant (54). Because of the number of markers involved in the construction of this strain, the wild-type copy of Sup35 was retained, and we examined only newly assembled NM dot structures, induced with a galactose-inducible NM-YFP construct (18). Gold-labeled anti-YFP antibodies were used to identify prion dot assemblies in freeze-substituted EM sections with and without the additional ts mutation in Ssa1, both at 25 °C and after a shift to 37 °C. The organization of fiber arrays was disturbed in the strain with the Ssa1-ts mutation, compared with cells with wild-type SSA1. The fibril bundles were more disorganized, especially after the shift to 37 °C (Fig. S2 *B–D*).

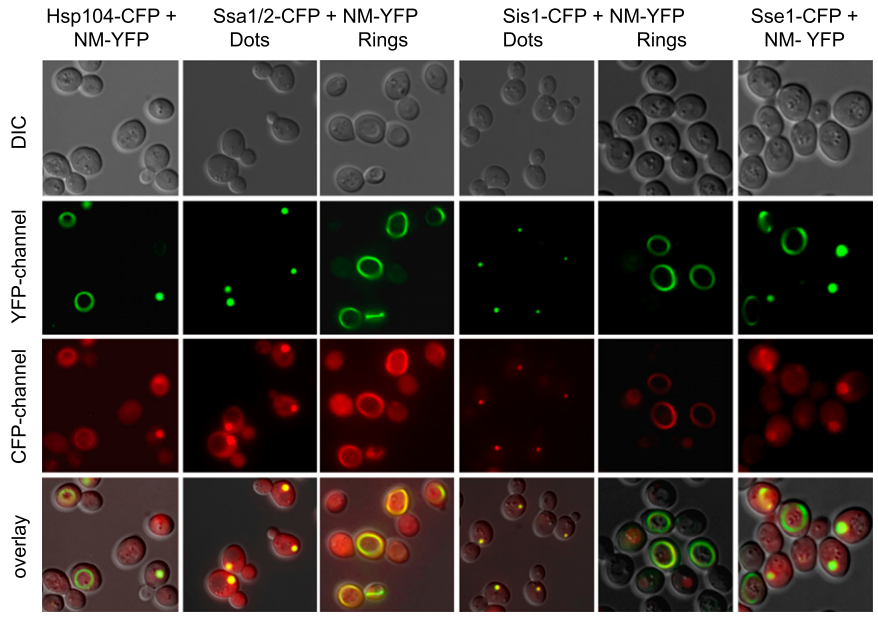

Fig. 4. Fluorescence microscopy showing colocalization of chaperones with NM-YFP in ring and dot structures. DIC, differential interference contrast images. The prion fibers are labeled with YFP (NM-YFP), and the chaperones are labeled with CFP. The results show that Hsp104, the Hsp70 proteins Ssa1/2 and Sse1, and the Hsp40 protein Sis1 are all found in dots and rings.

Discussion

The yeast prion phenomenon is of much broader importance in biology than was initially anticipated (3, 4, 8, 10, 12, 17). Despite recent advances in characterizing prions and the biochemistry of their propagation (4, 5, 11, 19, 20), little is known about the cellular organization of amyloid fibers in these protein-based elements of inheritance. A growing body of evidence suggests that prion amyloid assemblies, like other amyloids, are deposited at distinct protein quality control sites, particularly for abundant species (12, 35–37, 46). Such deposition could serve to sequester potentially damaging aggregates for retention in the mother cell, a common principle also observed for oxidatively damaged proteins during cell division, with implications for cellular aging (55). However, despite retention of prion aggregates at the IPOD, sufficient amounts of seeds are transmitted to daughter cells to faithfully propagate the prion state (35, 40, 41). Therefore, deposition and transmission of prion aggregates must be regulated, a process likely to involve specific organization of prion fibrils by cellular factors.

How can a cell achieve such a high degree of order for amyloid deposits as observed previously (35, 41) and in greater detail in this study? NM fibers have never been observed to form such arrays in vitro (22, 27, 49, 52). Therefore, we reasoned that other cellular factors must dictate the arrangement of the fibril arrays. The 10-nm diameter of the fibers observed in our cryo–electron tomography studies is consistent with that of fibers generated in vitro from NM or N alone (22, 49). Subtomogram averaging identified elongated structures intercalated at semiregular positions along and between the fibrils that could explain their wide, parallel spacing.

What could be forming these 8- to 9-nm densities? Various studies have shown molecular chaperones coprecipitating with [*PSI*$^+$] prion aggregates (32, 34, 35). Indeed, we found colocalization of several molecular chaperones including Hsp104, Ssa1/2, and Sis1 with the prion assemblies by fluorescence microscopy (Fig. 4). Ssa1 appeared particularly abundant in the assemblies, consistent with previous copurification of Ssa1/2 with [*PSI*$^+$] prion aggregates in a nearly 1:1 ratio (34). The presence of molecular chaperones is likely related to their roles in remodeling of prion aggregates and propagation of the prion state (31, 50, 56). Indeed, Hsp104 (26) and Sis1, a cochaperone of Ssa, play essential roles in severing of [*PSI*$^+$] prion fibers during the prion-propagation cycle, likely in cooperation with Ssa (44, 51). Given the high abundance of Ssa1/2 in prion aggregates relative to other factors required for fiber severing, e.g., Hsp104 (34), it may serve an additional function. A recent study of a ribosome-associated Hsp70-40 complex, Ssz–zuotin, suggests an end-to-end binding of these two components, which could generate an extended assembly (57). By analogy, elongated structures could be formed by Ssa1/2 and Sis1, and either serve a scaffolding function and/or regulate access of other factors, thereby influencing the processing of prion fibrils. Furthermore, overexpression of Ssa1/2 in [*PSI*$^+$] cells expressing a construct with GFP incorporated into the endogenous copy of SUP35 between the N and M domains causes a shift from multiple small aggregates to fewer, larger ones (58). This phenotype may also hint at a role of Ssa1/2 in organization of prion aggregates.

Indeed, in an initial approach, deleting all functional copies of Ssa (54) from cells displaying dots caused some disruption to the prion fibril assemblies (Fig. S2 *C* and *D*). At this point, we cannot distinguish whether the effect observed in cells with reduced Ssa is directly or indirectly attributable to the loss of Ssa function. Thus, the present results raise the possibility that the Hsp70 system organizes fibril deposition in NM dots. However, it is not currently possible to directly identify the interfibril structures, which are packed too closely to be discriminated from the fibrils by immuno-EM.

Further analysis is needed to confirm this hypothesis and to establish how these ordered prion fiber assemblies are formed in yeast cells. The appearance of similar ring and dot structures for other prion-like proteins (12, 36, 47) raises the possibility that the amyloid fiber organization in highly ordered arrays is a common principle for units of protein-based inheritance.

Materials and Methods

Yeast Strains, Constructs, Media, and Fluorescence Microscopy. Yeast strains, constructs, media, and fluorescence microscopy were performed as described in refs. 18, 35, and 54 and in *SI Materials and Methods*.

EM Sample Preparation and Data Collection. Cells were high-pressure–frozen in an EMPACT 2 freezer and freeze-substituted into Lowicryl HM20 (Polysciences) following the protocol of Hawes et al. (59) with 0.2% or 2% (wt/vol) uranyl acetate, or with 0.2% glutaraldehyde, 0.1% uranyl acetate and 1% (vol/vol) water in acetone. The electron micrographs were recorded on a 2,000 × 2,000 pixel CCD camera with a pixel size at the specimen level between 0.6 and 1 nm. The total electron dose applied on the cryosamples was around 70 e/Å^2.

Image Processing. Alignment of the room temperature tomograms was done with etomo (60) using the gold particles as fiducial markers, whereas the cryotomograms were aligned by cross-correlation (61).

ACKNOWLEDGMENTS. We thank Ashraf Al-Amoudi for help with sample preparation and EM; Jamie Riches, Simone Prinz, and John Briggs for helpful advice and discussions; Silke Druffel-Augustin for cloning of NM with small epitope tags; Zhou Yu for help with figures; and Dieter Wolf for providing the Ssa deletion strain. This work was funded, in part, by the Howard Hughes Medical Institute (HHMI). S.L. is an investigator of the HHMI. We thank the Wellcome Trust and Leverhulme Trust for sabbatical fellowships to H.R.S., the European Research Council (ERC) for a starting grant to A.S.F., and the Deutsche Forschungsgemeinschaft (DFG) for a grant to J.T. (TY93/1-1).

1. Collinge J, Clarke AR (2007) A general model of prion strains and their pathogenicity. *Science* 318:930–936.
2. Polymenidou M, Cleveland DW (2011) The seeds of neurodegeneration: Prion-like spreading in ALS. *Cell* 147:498–508.
3. Halfmann R, Lindquist S (2010) Epigenetics in the extreme: Prions and the inheritance of environmentally acquired traits. *Science* 330:629–632.
4. Tuite MF, Serio TR (2010) The prion hypothesis: From biological anomaly to basic regulatory mechanism. *Nat Rev Mol Cell Biol* 11:823–833.
5. Shorter J, Lindquist S (2005) Prions as adaptive conduits of memory and inheritance. *Nat Rev Genet* 6:435–450.
6. Si K, Choi YB, White-Grindley E, Majumdar A, Kandel ER (2010) Aplysia CPEB can form prion-like multimers in sensory neurons that contribute to long-term facilitation. *Cell* 140:421–435.
7. Hou F, et al. (2011) MAVS forms functional prion-like aggregates to activate and propagate antiviral innate immune response. *Cell* 146:448–461.
8. Halfmann R, et al. (2012) Prions are a common mechanism for phenotypic inheritance in wild yeasts. *Nature* 482:363–368.
9. True HL, Lindquist SL (2000) A yeast prion provides a mechanism for genetic variation and phenotypic diversity. *Nature* 407:477–483.
10. Jarosz DF, Taipale M, Lindquist S (2010) Protein homeostasis and the phenotypic manifestation of genetic diversity: Principles and mechanisms. *Annu Rev Genet* 44: 189–216.
11. Tuite MF, Marchante R, Kushnirov V (2011) Fungal prions: Structure, function and propagation. *Top Curr Chem* 305:257–298.
12. Alberti S, Halfmann R, King O, Kapila A, Lindquist S (2009) A systematic survey identifies prions and illuminates sequence features of prionogenic proteins. *Cell* 137: 146–158.
13. Chernoff YO, et al. (2000) Evolutionary conservation of prion-forming abilities of the yeast Sup35 protein. *Mol Microbiol* 35:865–876.
14. Zenthon JF, Ness F, Cox B, Tuite MF (2006) The [PSI+] prion of Saccharomyces cerevisiae can be propagated by an Hsp104 orthologue from Candida albicans. *Eukaryot Cell* 5:217–225.
15. Harrison LB, Yu Z, Stajich JE, Dietrich FS, Harrison PM (2007) Evolution of budding yeast prion-determinant sequences across diverse fungi. *J Mol Biol* 368:273–282.
16. Sideri TC, Stojanovski K, Tuite MF, Grant CM (2010) Ribosome-associated peroxiredoxins suppress oxidative stress-induced de novo formation of the [PSI+] prion in yeast. *Proc Natl Acad Sci USA* 107:6394–6399.
17. Suzuki G, Shimazu N, Tanaka M (2012) A yeast prion, Mod5, promotes acquired drug resistance and cell survival under environmental stress. *Science* 336:355–359.
18. Tyedmers J, Madariaga ML, Lindquist S (2008) Prion switching in response to environmental stress. *PLoS Biol* 6:e294.
19. Shkundina IS, Ter-Avanesyan MD (2007) Prions. *Biochemistry (Mosc)* 72:1519–1536.
20. Chernoff YO (2007) Stress and prions: Lessons from the yeast model. *FEBS Lett* 581: 3695–3701.
21. Patino MM, Liu JJ, Glover JR, Lindquist S (1996) Support for the prion hypothesis for inheritance of a phenotypic trait in yeast. *Science* 273:622–626.
22. Glover JR, et al. (1997) Self-seeded fibers formed by Sup35, the protein determinant of [PSI+], a heritable prion-like factor of S. cerevisiae. *Cell* 89:811–819.
23. King CY, Diaz-Avalos R (2004) Protein-only transmission of three yeast prion strains. *Nature* 428:319–323.
24. Tanaka M, Chien P, Naber N, Cooke R, Weissman JS (2004) Conformational variations in an infectious protein determine prion strain differences. *Nature* 428:323–328.
25. Li L, Lindquist S (2000) Creating a protein-based element of inheritance. *Science* 287: 661–664.
26. Chernoff YO, Lindquist SL, Ono B, Inge-Vechtomov SG, Liebman SW (1995) Role of the chaperone protein Hsp104 in propagation of the yeast prion-like factor [psi+]. *Science* 268:880–884.
27. Shorter J, Lindquist S (2004) Hsp104 catalyzes formation and elimination of self-replicating Sup35 prion conformers. *Science* 304:1793–1797.
28. Paushkin SV, Kushnirov VV, Smirnov VN, Ter-Avanesyan MD (1996) Propagation of the yeast prion-like [psi+] determinant is mediated by oligomerization of the SUP35-encoded polypeptide chain release factor. *EMBO J* 15:3127–3134.
29. Wegrzyn RD, Bapat K, Newnam GP, Zink AD, Chernoff YO (2001) Mechanism of prion loss after Hsp104 inactivation in yeast. *Mol Cell Biol* 21:4656–4669.
30. Ness F, Ferreira P, Cox BS, Tuite MF (2002) Guanidine hydrochloride inhibits the generation of prion "seeds" but not prion protein aggregation in yeast. *Mol Cell Biol* 22:5593–5605.
31. Satpute-Krishnan P, Langseth SX, Serio TR (2007) Hsp104-dependent remodeling of prion complexes mediates protein-only inheritance. *PLoS Biol* 5:e24.
32. Allen KD, et al. (2005) Hsp70 chaperones as modulators of prion life cycle: Novel effects of Ssa and Ssb on the Saccharomyces cerevisiae prion [PSI+]. *Genetics* 169: 1227–1242.
33. Ganusova EE, et al. (2006) Modulation of prion formation, aggregation, and toxicity by the actin cytoskeleton in yeast. *Mol Cell Biol* 26:617–629.
34. Bagriantsev SN, Gracheva EO, Richmond JE, Liebman SW (2008) Variant-specific [PSI+] infection is transmitted by Sup35 polymers within [PSI+] aggregates with heterogeneous protein composition. *Mol Biol Cell* 19:2433–2443.
35. Tyedmers J, et al. (2010) Prion induction involves an ancient system for the sequestration of aggregated proteins and heritable changes in prion fragmentation. *Proc Natl Acad Sci USA* 107:8633–8638.
36. Mathur V, Taneja V, Sun Y, Liebman SW (2010) Analyzing the birth and propagation of two distinct prions, [PSI+] and [Het-s](y), in yeast. *Mol Biol Cell* 21:1449–1461.
37. Chernova TA, et al. (2011) Prion induction by the short-lived, stress-induced protein Lsb2 is regulated by ubiquitination and association with the actin cytoskeleton. *Mol Cell* 43:242–252.
38. Tyedmers J (2012) Patterns of [PSI(+)] aggregation allow insights into cellular organization of yeast prion aggregates. *Prion* 6:191–200.
39. Zhou P, Derkatch IL, Liebman SW (2001) The relationship between visible intracellular aggregates that appear after overexpression of Sup35 and the yeast prion-like elements [PSI(+)] and [PIN(+)]. *Mol Microbiol* 39:37–46.
40. Kawai-Noma S, et al. (2006) Dynamics of yeast prion aggregates in single living cells. *Genes Cells* 11:1085–1096.
41. Kawai-Noma S, et al. (2010) In vivo evidence for the fibrillar structures of Sup35 prions in yeast cells. *J Cell Biol* 190:223–231.
42. Osherovich LZ, Weissman JS (2001) Multiple Gln/Asn-rich prion domains confer susceptibility to induction of the yeast [PSI(+)] prion. *Cell* 106:183–194.
43. Cox B, Ness F, Tuite M (2003) Analysis of the generation and segregation of propagons: Entities that propagate the [PSI+] prion in yeast. *Genetics* 165:23–33.
44. Tipton KA, Verges KJ, Weissman JS (2008) In vivo monitoring of the prion replication cycle reveals a critical role for Sis1 in delivering substrates to Hsp104. *Mol Cell* 32: 584–591.
45. Vishveshwara N, Bradley ME, Liebman SW (2009) Sequestration of essential proteins causes prion associated toxicity in yeast. *Mol Microbiol* 73:1101–1114.
46. Kaganovich D, Kopito R, Frydman J (2008) Misfolded proteins partition between two distinct quality control compartments. *Nature* 454:1088–1095.
47. Derkatch IL, Bradley ME, Hong JY, Liebman SW (2001) Prions affect the appearance of other prions: The story of [PIN(+)]. *Cell* 106:171–182.
48. Al-Amoudi A, Norlen LP, Dubochet J (2004) Cryo-electron microscopy of vitreous sections of native biological cells and tissues. *J Struct Biol* 148:131–135.
49. Baxa U, Keller PW, Cheng N, Wall JS, Steven AC (2011) In Sup35p filaments (the [PSI+] prion), the globular C-terminal domains are widely offset from the amyloid fibril backbone. *Mol Microbiol* 79:523–532.
50. Song Y, et al. (2005) Role for Hsp70 chaperone in Saccharomyces cerevisiae prion seed replication. *Eukaryot Cell* 4:289–297.
51. Higurashi T, Hines JK, Sahi C, Aron R, Craig EA (2008) Specificity of the J-protein Sis1 in the propagation of 3 yeast prions. *Proc Natl Acad Sci USA* 105:16596–16601.
52. Krzewska J, Melki R (2006) Molecular chaperones and the assembly of the prion Sup35p, an in vitro study. *EMBO J* 25:822–833.
53. Shorter J, Lindquist S (2008) Hsp104, Hsp70 and Hsp40 interplay regulates formation, growth and elimination of Sup35 prions. *EMBO J* 27:2712–2724.
54. Becker J, Walter W, Yan W, Craig EA (1996) Functional interaction of cytosolic hsp70 and a DnaJ-related protein, Ydj1p, in protein translocation in vivo. *Mol Cell Biol* 16: 4378–4386.
55. Aguilaniu H, Gustafsson L, Rigoulet M, Nyström T (2003) Asymmetric inheritance of oxidatively damaged proteins during cytokinesis. *Science* 299:1751–1753.
56. Kryndushkin DS, Alexandrov IM, Ter-Avanesyan MD, Kushnirov VV (2003) Yeast [PSI+] prion aggregates are formed by small Sup35 polymers fragmented by Hsp104. *J Biol Chem* 278:49636–49643.
57. Fiaux J, et al. (2010) Structural analysis of the ribosome-associated complex (RAC) reveals an unusual Hsp70/Hsp40 interaction. *J Biol Chem* 285:3227–3234.
58. Mathur V, Hong JY, Liebman SW (2009) Ssa1 overexpression and [PIN(+)] variants cure [PSI(+)] by dilution of aggregates. *J Mol Biol* 390:155–167.
59. Hawes P, Netherton CL, Mueller M, Wileman T, Monaghan P (2007) Rapid freeze-substitution preserves membranes in high-pressure frozen tissue culture cells. *J Microsc* 226:182–189.
60. Mastronarde DN (1997) Dual-axis tomography: An approach with alignment methods that preserve resolution. *J Struct Biol* 120:343–352.
61. Castaño-Díez D, Scheffer M, Al-Amoudi A, Frangakis AS (2010) Alignator: A GPU powered software package for robust fiducial-less alignment of cryo tilt-series. *J Struct Biol* 170:117–126.